

# PCCCP

Physical Chemistry Chemical Physics

Accepted Manuscript

This article can be cited before page numbers have been issued, to do this please use: M. Al Huwayz, D. A. Jameel, W. M. Azevedo, J. Felix, N. A. Al Saqri, O. M. Lemine, S. N. A. Abu Alrub and M. Henini, *Phys. Chem. Chem. Phys.*, 2023, DOI: 10.1039/D3CP03865C.



This is an Accepted Manuscript, which has been through the Royal Society of Chemistry peer review process and has been accepted for publication.

Accepted Manuscripts are published online shortly after acceptance, before technical editing, formatting and proof reading. Using this free service, authors can make their results available to the community, in citable form, before we publish the edited article. We will replace this Accepted Manuscript with the edited and formatted Advance Article as soon as it is available.

You can find more information about Accepted Manuscripts in the [Information for Authors](#).

Please note that technical editing may introduce minor changes to the text and/or graphics, which may alter content. The journal's standard [Terms & Conditions](#) and the [Ethical guidelines](#) still apply. In no event shall the Royal Society of Chemistry be held responsible for any errors or omissions in this Accepted Manuscript or any consequences arising from the use of any information it contains.

# Effects of Gamma Radiation on the Electrical Properties of InAs/InGaAs Quantum Dots Based Laser Structures Grown on GaAs and Si Substrates by Molecular Beam Epitaxy

M. Al Huwayz<sup>1,2</sup>, D. A. Jameel<sup>3</sup>, Walter M. de Azevedo<sup>4</sup>, Jorlandio F. Felix<sup>5</sup>, N. Al Saqri<sup>6</sup>, O. M. Lemine<sup>7</sup>, S. Abu Alrub<sup>7</sup>, M. Henini<sup>2</sup>

<sup>1</sup>*Department of Physics, College of Sciences, Princess Nourah bint Abdulrahman University (PNU), Riyadh, 11671, Saudi Arabia*

<sup>2</sup>*School of Physics and Astronomy, University of Nottingham, Nottingham, NG7 2RD, UK*

<sup>3</sup>*Department of General Sciences, College of Basic Education, University of Zakho, Zakho, Kurdistan Region Iraq, Iraq*

<sup>4</sup>*Departamento de Química Fundamental, Universidade Federal de Pernambuco (UFPE), 50740-560, Recife/PE, Brazil*

<sup>5</sup>*Institute of Physics, NFA, University of Brasilia (UnB), Brasilia, DF, 70910-900, Brazil*

<sup>6</sup>*Department of Physics, College of Science, Box 36, Sultan Qaboos University, Al Khoud 123, Oman*

<sup>7</sup>*Department of Physics, College of Sciences, Imam Mohammad Ibn Saud Islamic University (IMISU), Riyadh 11623, Saudi Arabia*

\* [dler.jameel@uoz.edu.krd](mailto:dler.jameel@uoz.edu.krd)

## Abstract

This study investigates the impact of gamma radiation on the electrical properties of InAs/InGaAs quantum dots based laser structures grown on both GaAs (Sample A) and Si (Sample B) substrates using molecular beam epitaxy. The research explores the electrical characteristics of the lasers before and after being exposed to gamma radiation employing Current - Voltage (I-V), Capacitance - Voltage (C-V), Deep Level Transient Spectroscopy (DLTS) and Laplace DLTS techniques. The results show that the electrical properties of the lasers change due to gamma radiation exposure, and the extent of the change depends on the substrate used for growth. The I-V results revealed that the ideality factor ( $n$ ) and built-in voltage were increased in Sample A and Sample B after radiation. Nonetheless, the series resistance ( $R_s$ ) at room temperature decreased in both samples after radiation. Overall, this study provides valuable insights into the effects of gamma radiation on the electrical properties of InAs/InGaAs quantum dots lasers and highlights the importance of considering substrate materials in the design of radiation-hardened electronic devices.

**Keywords:** InAs quantum dots (QDs), Gamma radiation, GaAs, Si, I-V, C-V, DLTS

## 1 Introduction

View Article Online  
DOI: 10.1039/D3CP03865C

Within the field of QDs systems the area of InAs QDs has attracted much research activity, which is due to the possibility of achieving light emission covering the optical communication wavelength bands [1]–[3]. The study of the electrical properties of any semiconductor materials is important in order to understand the possibility of using them in different electronic and optoelectronic applications. Electrical properties of PN junctions and Schottky diodes are affected by a multitude of factors. These include interface chemistry, processing methodology, the existence of native defects referred to as interface states and doping concentration of the semiconductor [4]. In addition, modifying the atomic configuration and inducing other defects into the lattice has been found to take place through exposure of semiconductor materials to radiation, which consequently changes their electrical and optical properties [4], [5]. It is therefore important to investigate the effect of radiation on the performance of semiconductor-based devices such as Schottky diodes, solar cells, lasers, heterostructures and metal-insulator/oxide-semiconductors due to the fact that they are used in satellites. A significant number of lattice defects are produced in semiconductors as a result of radiation in space, which reduce the devices' performance [6], [7]. Moreover, the study of the defects induced by radiation led to better devices used in space which are more radiation-resistant.

To investigate the effect of electron irradiation and proton hydrogenation on the electrical properties of GaAsN devices grown by Chemical Beam Epitaxy (CBE) on the main nitrogen-related nonradiative recombination center E1 which has activation energy of 0.33 eV below the bottom edge of the conduction band, B. Bouzazi *et al.* [8] employed Deep Level Transient Spectroscopy (DLTS) technique. Their study proposed that the origin of this defect is related to the compensation of the tensile strain in the film produced by the small atomic size of N atom compared to that of As. In addition, the density of E1 increased with increasing the fluency doses of electron irradiation [8].

Furthermore, the effect of gamma irradiation on the electron traps present in as-grown liquid encapsulated Czochralski GaAs was described by T. Hashizume and H. Hasegawa [5]. They discovered that following irradiation, the concentration of EL6 (0.35 eV) trap was reduced by a factor of 3-5, whereas the density of EL3 (0.56 eV) increased by a factor of one order of magnitude [5], [9].

The effect of gamma irradiation on dilute GaAsN layers with different nitrogen concentrations ranging from 0.2 to 1.2% grown on n+ GaAs substrates by Molecular Beam Epitaxy (MBE) was investigated by N. Al Saqri et al. [10] by using DLTS and Laplace DLTS (LDLTS) techniques. According to their study, the number of traps either decreased, remained the same or new traps were created after irradiation depending on the nitrogen content.

This paper presents an experimental investigation on the effect of gamma irradiation on InAs/InGaAs QD lasers grown on GaAs and Si substrates using Current - Voltage (I-V), Capacitance - Voltage (C-V), Deep Level Transient Spectroscopy (DLTS) and Laplace DLTS measurements techniques. The experimental results showed that gamma irradiation improves the electrical properties of the devices, due the reduction of the concentration of the defects and/or their transformation.

## 2 Sample details

In this work, the samples investigated are p-i-n laser diodes with InAs self-assembled quantum dots (QDs) incorporated in the i-region. The samples were fabricated using the same technique as reported in reference [11], [12]. In summary, the InAs QDs laser are deposited on (100) n-type GaAs (Sample A: control sample) and (100) n-type Si substrates (Sample B). The Sample A consists of the following layers: a 50 nm n-GaAs buffer, a thin film of 1500 nm  $\text{Al}_{0.42}\text{Ga}_{0.58}\text{As}$  covering layer, a 108 nm undoped GaAs spacer layer,  $4 \times [2.5 \text{ monolayers (MLs)} \text{ InAs QDs}/10 \text{ nm } \text{In}_{0.15}\text{Ga}_{0.85}\text{As}$  (strain reducing layer, SRL)/40 nm GaAs/10 nm  $\text{In}_{0.15}\text{Ga}_{0.85}\text{As}$

(SRL)], a 64 nm undoped GaAs spacer layer, a 1500 nm p-Al<sub>0.42</sub>Ga<sub>0.58</sub>As cladding layer, and a thin film of 300 nm p-GaAs. The InAs QDs was deposited at a temperature of 500 °C and a growth rate of 0.03 monolayer ML/s. Before the growth of the 6 nm of In<sub>0.15</sub>Ga<sub>0.85</sub>As SRL followed by 10 nm thick of GaAs layers, a short deposition interruption under As<sub>2</sub> flux was introduced. Subsequently, the growth temperature was increased to 570 °C to deposit the remaining GaAs cap layer. The covering, contacts, and spacers' layers were deposited at 570 °C.

The layers of sample B, grown on n-type Si substrate, were grown utilizing the same technique and growth conditions as used for sample A except for the buffer layer which is designed and utilized to reduce the defects produced from the lattice mismatch between Si and GaAs substrates. Finally, the Ohmic contacts were obtained by thermal evaporation of 99.99% Au on the p+ GaAs films with the area of  $2.83 \times 10^{-3} \text{ cm}^2$  for Sample A: as-grown, Sample A: irradiated and Sample B: as-grown; and area of  $5.02 \times 10^{-3} \text{ cm}^2$  for Sample B: irradiated. The I–V measurements were performed utilizing current–voltage (I–V) source-meter unit (model Keithley 236) and a closed-loop helium cryostat model CCS-450 (Janis Research Company). The capacitance–voltage (C–V) measurements were done employing an LCR meter (Agilent E4980A). Finally, the temperature-dependent DLTS and LDLTS measurements have been carried out on all the samples using a temperature controller (Lake Shore 331), capacitance meter (Boonton 7200) and a pulse generator (Agilent 33220A). To investigate the impact of radiation on the InAs QDs laser structures grown on n-type GaAs and Si substrates, the samples were irradiated with a gamma cell Cobalt Irradiator (dose rate of 5.143 kGys/hour) at a high dose of 50 kGy.

### 3 Results and discussion

#### 3.1 Current-Voltage (I-V) measurements

In order to investigate the effect of gamma irradiation on the electrical properties of InAs/InGaAs QDs laser structures grown on GaAs (Sample A) and Si (Sample B) substrates, I-V measurements at different temperatures were performed. Figure 1(a) and Figure 2(a) illustrate the current–voltage (I–V) characteristics at room temperature of Sample A and Sample B, respectively, before and after irradiation. However, due to the different areas of the samples and for comparison purposes, the current density (J) versus reverse bias is plotted for both samples as shown in Figure 1(b) and Figure 2(b).

As shown in Figure 1(b), the J-V characteristics of Sample A improved after irradiation. The reverse current of the irradiated Sample A is lower than that of the as-grown Sample A. On the other hand, since the contact areas of as-grown Sample B (effective diode area  $A = 2.83 \times 10^{-3} \text{ cm}^2$ ) and irradiated ( $A = 5.02 \times 10^{-3} \text{ cm}^2$ ) are different, the current density (J) is plotted in Figure 2 instead of current (I). As clearly seen in Figure 2, Sample B grown on Si substrates also exhibited lower reverse currents after irradiation. However, the decrease in reverse current density after irradiation is larger for Sample A. For example, at  $V_R = -1\text{V}$ , the current density in Sample A decreased from  $1.04 \times 10^{-3} \text{ A}$  to  $8.04 \times 10^{-5} \text{ A}$  after irradiation, while at the same reverse voltage, the current density of Sample B decreased from  $1.28 \times 10^{-4} \text{ Acm}^{-2}$  to  $1.57 \times 10^{-5} \text{ Acm}^{-2}$ . This decrease in reverse current after irradiation in both Sample A and Sample B may indicate that the density of the defects in as-grown samples decreased and/or the number of defects changed by annihilation or generation. In addition, the deep level defects can act as generation recombination centers and most likely they will play a role in carrier recombination in the reverse current characteristics [13], [14].

In order to study the electrical parameters of the diodes such as ideality factor ( $n$ ), built-in potential ( $V_{bi}$ ), and series resistance ( $R_s$ ), the thermionic emission equation [15] was used, which is represented by:

$$J = J_s \left[ \exp\left(\frac{q(V - JR_s)}{nkT}\right) - 1 \right] \quad (1)$$

where  $J_s$  is saturation current density and is expressed by:

$$J_s = A^{**} T^2 \exp\left(\frac{-qV_{bi}}{kT}\right) \quad (2)$$

In the above equations,  $q$  is the electronic charge,  $V$  is the applied voltage,  $T$  is the absolute temperature in Kelvin,  $k_B$  is the Boltzmann constant,  $A^{**}$  is the effective Richardson's constant for a semiconductor material and  $A$  is the diode area.

The enhanced Werner's approach was used to increase the precision of the characteristic parameters ( $n$ ,  $V_{bi}$ , and  $R_s$ ) of the devices [16]. The values of  $n$ ,  $V_{bi}$ , and  $R_s$  over the temperature 160 - 420 K were obtained. The J-V characteristics for all samples were analysed further to understand their properties by calculating the local ideality factor,  $n(V)$ , using the following approximation equation [17], [18].

$$n(V) = \frac{d(V/V_t)}{d[\ln(J/J_s)]} \quad (3)$$

where  $V_t$  is the thermal voltage, which is given by  $V_t = k_B T/q$ .

The local ideality factors for all samples are calculated at room temperature and their values change with voltage as shown in Figure 3. As can be seen from Figure 3, for each device there are two noticeable behaviours observed at low voltage ( $\sim 0.08$  V) and high voltage (0.3 V) regions. In particular, at high voltages Sample A exhibit a clear peak before and after irradiation. In addition, irradiated Sample A shows a pronounced peak at low voltages.

However, for Sample B these peaks are less significant at low voltages and absent at high voltages for both as-grown and irradiated devices. This behaviour of the local ideality factor could indicate that there are different conduction mechanisms occurring in the investigated devices [17], [18]. Moreover, in all samples the values of the ideality factor ( $n$ ) are greater than unity for voltages greater than  $\sim 0.05$  V, indicating carrier recombination mechanisms such as band-to-band radiative recombination, Shockley-Read-Hall recombination (also called trap-assisted recombination) through defects, and defect-assisted tunnelling or surface recombination [19], [20]. These processes could possibly explain the large ideality factors observed in these samples which incorporate QDs in the intrinsic region and which create an additional current component that contributes to the total current of the devices. It is worth pointing out that Sample B (as-grown and irradiated) has a different trend at high voltage ranges (i.e., no peak is observed) which suggests that some mechanisms are presumably suppressed or enhanced by growing on Si substrates, and some of the mechanisms are possibly unique to the devices grown on Si.

Table 1 summarises the electrical parameters of the diodes at room temperature. As-grown Sample A has a lower ideality factor ( $n = 1.54$ ), a slightly lower built-in potential energy ( $V_{bi} = 0.63$  eV) and a higher series resistance ( $R_s = \sim 221$  k $\Omega$ ) when compared to irradiated Sample A ( $n = 1.86$ ;  $V_{bi} = 0.74$  eV;  $R_s = \sim 20 \times 10^{-3}$  k $\Omega$ ). Likewise, as-grown Sample B has a slightly lower value of ideality factor ( $n = 1.70$ ), lower built-in potential energy ( $V_{bi} = 0.63$  eV) and slightly larger series resistance ( $R_s = \sim 2.31 \times 10^{-3}$  k $\Omega$ ) when compared to irradiated Sample B ( $n = 1.73$ ;  $V_{bi} = 0.67$  eV;  $R_s = \sim 3.5 \times 10^{-4}$  k $\Omega$ ). At room temperature, both as-grown samples have ideality factors close to unity, whereas a deviation of  $n$  from unity can indicate that the conduction mechanism can be dominated by diffusion mechanism (thermionic emission) and

other factors such as series resistance, interface states, generation-recombination mechanism [21]–[24].

Figures 4, 5 and 6 show the behaviours of built-in potential energy ( $V_{bi}$ ), series resistance ( $R_s$ ) and ideality factor ( $n$ ) as a function of temperature, respectively, for Sample A and Sample B before and after irradiation. As shown in Figure 4, the built-in potential energy increases with increasing temperature before and after radiation for Sample A. This temperature dependence of the built-in potential energy is due to the effect of potential inhomogeneities at the p-i-n interface [25]. The built-in potential energy of Sample A after irradiation increased for all temperatures as compared to the as-grown sample. Similar trend was observed for irradiated Sample B for temperatures up to  $\sim 280\text{K}$ , but for temperatures  $> \sim 280\text{K}$   $V_{bi}$  of as-grown and irradiated Sample B was similar.

Figure 5 shows the dependence of the series resistance as a function of temperature of Sample A and Sample B before and after irradiation. As shown in Figure 5, this behaviour is different for both samples. The series resistance of as-grown Sample A, which decreased with increasing temperature, became very small and practically independent of temperature. However, for Sample B, the low and temperature insensitive series resistance of the as-grown structure, showed a decaying behaviour with increasing temperature after irradiation. In addition, it can be seen from Figure 5 that the resistance of Sample A and Sample B change rapidly with temperature. These results are associated with gamma radiation which has the capability to cause an increase in temperature, thereby inducing structural alterations in the multilayer materials. In this scenario, gamma radiation may initiate a form of thermal annealing, inducing a process of activation of dopants, in turn, contributes to the improvement of electrical properties of devices.

The ideality factor of the irradiated samples A and B became more uniform and did not change very much for temperatures greater than  $\sim 225$  K and  $\sim 275$  K, respectively, as shown in Figure 6. However, the ideality factor of samples A and B were smaller after irradiation for temperatures lower than 200 K and 250 K, respectively.

### 3.2 Capacitance-Voltage (C-V) measurements

C-V measurements were recorded at room temperature utilizing a BOONTON 7200 capacitance meter to determine the free carrier concentration ( $N_d$ ) of both samples. Figure 8.7(a) and 8.8(a) illustrate the capacitance-voltage (C-V) characteristics at room temperature of Sample A and Sample B, respectively, before and after irradiation. On the other hand, due to the difference in the area of the samples, the change of capacitance per area at room temperature as a function of reverse bias of all samples is plotted as shown in Figures 7(b) and 8(b) for comparison purposes. Figures 7(a) and 7(b) show that the change of capacitance is similar for Sample A before and after irradiation. The capacitance of as-grown and irradiated Sample B also follows a similar trend as shown in Figures 8(a) and 8(b), respectively. As clearly seen in Figures 7 and 8 the capacitance of both Sample A and Sample B decreases after irradiation. However, the decrease in capacitance/area is more pronounced in the irradiated Sample A than in irradiated Sample B.

It is important to note from Figures 7 and 8 that after irradiation, the capacitance values decreased in all samples. This decrease can be attributed to the dielectric constant change at the p-i-n interface and/or the reduction of net ionized dopant concentration due to the capture of charge carriers by defects [26]–[28].

On the other hand, as can be noticed in Figure 9, the plots of  $1/C^2$  versus reverse bias V for all samples at room temperature are nonlinear revealing that the junction doping profile (concentration of carriers as a function of depletion width) are neither uniform nor linearly

graded [29], i.e. they are not abrupt. These results for all samples infer non-uniformity in the carrier distribution at the interface and away from the interface. These effects could cause a non-homogeneous or a spatially distributed barrier potential at the interface. As a result, the gamma radiation dose does not impact on the junction doping profiles.

### 3.3 DLTS and LDLTS measurements

DLTS and LDLTS measurements [30], [31] were performed in the temperature range of 20 - 440 K in both Samples A and B before and after irradiation in order to investigate the effect of gamma irradiation on deep-level defects at a filling pulse height  $V_p=0V$ , pulse width of  $t_p=1$  msec, rate window of  $200\text{ s}^{-1}$  and reverse bias of  $V_R = -4\text{ V}$ .

Figure 10(a, b) presents the DLTS spectra, before and after irradiation for both Sample A and Sample B with reverse bias of  $-4V$ . It can be seen that the DLTS signal of Sample A did not change after irradiation. Whereas the DLTS signal of Sample B increased by approximately half after irradiation.

Laplace DLTS was used to resolve the broader peaks observed in conventional DLTS. Figures 11 and 12 (a and b) show Arrhenius plots of  $\ln(e_n/T^2)$  vs  $(1000/T)$  for reverse bias of  $-4V$  for Sample A and Sample B before and after radiation.

The activation energy ( $E_T$ ), trap concentration ( $N_T$ ), and captured cross-section ( $\sigma_\infty$ ) of all defects detected were extracted from these plots and the DLTS/LDLTS spectra. Table 2 and Table 3 summarise these parameters.

Tables 2 and 3 show that the number of defects is larger in the samples grown on Si substrates. It is also important to note that in general, the defects detected in both samples (A

and B) after irradiation have different parameters than those observed in as-grown samples (A and B).

At  $V_R = -4V$ , the number of defects (i.e., number of trap energy levels) increased to two for both as-grown and irradiated Sample A. As-grown Sample A displayed two electron traps, namely  $EA1^{-4V}$  ( $0.05 \pm 0.01$  eV) and  $EA2^{-4V}$  ( $0.45 \pm 0.08$  eV). Likewise, irradiated Sample A presented two electron traps namely  $EA1_{Irrd}^{-4V}$  ( $0.21 \pm 0.02$  eV) and  $EA2_{Irrd}^{-4V}$  ( $0.22 \pm 0.01$  eV). However, as-grown Sample B has three electron traps  $EB1^{-4V}$  ( $0.0030 \pm 0.0002$  eV),  $EB2^{-4V}$  ( $0.067 \pm 0.003$  eV) and  $EB3^{-4V}$  ( $0.41 \pm 0.01$  eV), while the number of defect traps (i.e., number of trap energy levels) in irradiated Sample B decreased to two, namely  $EB1_{Irrd}^{-4V}$  ( $0.14 \pm 0.02$  eV) and  $EB2_{Irrd}^{-4V}$  ( $0.22 \pm 0.02$  eV).

In addition, at reverse bias voltage  $V_R = -4V$ , the traps  $EA2^{-4V}$  ( $0.45 \pm 0.08$  eV) and  $EB3^{-4V}$  ( $0.41 \pm 0.01$  eV) with similar activation energies and present in both as-grown samples (Sample A and Sample B) could also be of the same origin and attributed to  $EL5$  ( $\sim 0.43$  eV) which was assigned to complexes involving As interstitials- Ga vacancies ( $As_iV_{Ga}$ ) [32]. After irradiation this trap was annihilated in both samples, and new deep defects were created, namely  $EA2_{Irrd}^{-4V}$  and  $EB2_{Irrd}^{-4V}$ , with similar activation energies of  $\sim 0.22$  eV. These traps could be of the same origin, and could be related to  $EL10$  ( $\sim 0.18$  eV) [33] which was ascribed to an arsenic vacancy ( $V_{As}$ ) complex defect involving an impurity [34]–[36].

It is important to note that the shallow traps  $EA1^{-4V}$  ( $0.05$  eV),  $EB1^{-4V}$  ( $0.0030$  eV) and  $EB2^{-4V}$  ( $0.067$  eV) detected only in as-grown samples, have not been reported previously in the literature, and therefore their origins could not be identified in this work, but these could be related to shallow impurities introduced either intentionally or unintentionally. It is important to mention that no shallow defects were observed in irradiated samples.

In summary, the gamma radiation has an effect on the electrically active defects present in as-grown InAs/InGaAs QDs lasers grown on GaAs and Si substrates. This effect led to the number of traps either decreasing, remaining the same or new traps being created after irradiation.

## 4 Conclusion

I-V, C-V, DLTS and Laplace DLTS were used to investigate the effect of gamma irradiation on the electrical properties of InAs/InGaAs QD lasers grown on GaAs and Si substrates by MBE. From I-V measurements, the ideality factor ( $n$ ) and built-in voltage were increased in both samples after radiation. However, the series resistance ( $R_s$ ) at room temperature decreased in Sample A and Sample B after radiation.

In terms of the gamma radiation effect on the electrically active defects, the number of traps for Sample A was unchanged but the activation energies and traps' concentrations changed after irradiation. However, gamma radiation affected the electrically active defects of Sample B, in which the number of traps decreased from three to two traps. Moreover, the DLTS and Laplace DLTS have been able to reveal a close connection between the grown-in defects and those induced by radiation.

**Acknowledgements and Funding statement:** This work was supported and funded by the Deanship of Scientific Research at Imam Mohammad Ibn Saud Islamic University (IMSIU) (grant number IMSIU-RP23089). We thank Dr A. Salhi from Hamad Bin Khalifa University, Qatar, for providing the samples investigated in this work.

**Data access statement:** Data sets generated during the current study are available from the corresponding author on reasonable request.

**Ethics statement:** We, the authors of this paper, affirm our commitment to ethical research practices and have taken all necessary steps to ensure the credibility and validity of the results presented. This ethics statement serves as a testament to our dedication to upholding the highest ethical standards in scientific inquiry.

View Article Online  
DOI: 10.1039/C3CP03865C

practices and have taken all necessary steps to ensure the credibility and validity of the results presented. This ethics statement serves as a testament to our dedication to upholding the highest ethical standards in scientific inquiry.

## References

- [1] A. Creti *et al.*, "Role of charge separation on two-step two photon absorption in InAs/GaAs quantum dot intermediate band solar cells," *Appl. Phys. Lett.*, vol. 108, no. 6, 2016, doi: 10.1063/1.4941793.
- [2] M. V. Maksimov *et al.*, "High-power 1.5  $\mu\text{m}$  InAs-InGaAs quantum dot lasers on GaAs substrates," *Semiconductors*, vol. 38, no. 6, pp. 732–735, 2004, doi: 10.1134/1.1766381.
- [3] A. Salhi, S. Alshaibani, Y. Alaskar, A. Albadri, and A. Alyamani, "Achieving wavelength emission beyond the C-band from Type-II InAs-GaAsSb quantum dots grown monolithically on silicon substrate," *J. Alloys Compd.*, vol. 771, pp. 382–386, 2019, doi: 10.1016/j.jallcom.2018.08.276.
- [4] I. P. Vali *et al.*, "Gamma irradiation effects on Al/n-Si Schottky junction properties," *Nucl. Instruments Methods Phys. Res. Sect. B Beam Interact. with Mater. Atoms*, vol. 436, pp. 191–197, 2018, doi: 10.1016/j.nimb.2018.09.035.
- [5] T. Hashizume and H. Hasegawa, "Variation of deep electron traps created by  $\gamma$  irradiation of GaAs," *J. Appl. Phys.*, vol. 68, no. 9, pp. 4598–4603, 1990, doi: 10.1063/1.346168.
- [6] G. A. Umana-Membreno, J. M. Dell, G. Parish, B. D. Nener, L. Faraone, and U. K. Mishra, "<sup>60</sup>Co gamma irradiation effects on n-GaN Schottky diodes," *IEEE Trans. Electron Devices*, vol. 50, no. 12, pp. 2326–2334, Dec. 2003, doi: 10.1109/TED.2003.820122.
- [7] J. F. Felix *et al.*, "Effect of gamma radiation on the electrical properties of

- Polyaniline/silicon carbide heterojunctions,” *Radiat. Meas.*, vol. 71, pp. 402–406, 2014, doi: 10.1016/j.radmeas.2014.05.014.
- [8] B. Bouzazi, N. Kojima, Y. Ohshita, and M. Yamaguchi, “Effect of electron and proton irradiation on recombination centers in GaAsN grown by chemical beam epitaxy,” *Curr. Appl. Phys.*, vol. 13, no. 7, pp. 1269–1274, 2013, doi: 10.1016/j.cap.2013.03.017.
- [9] T. Richter, G. Kühnel, W. Siegel, and J. R. Niklas, “Activation energies of the EL6 trap and of the 0.15 eV donor and their correlation in GaAs,” *Semicond. Sci. Technol.*, vol. 15, no. 11, pp. 1039–1044, 2000, doi: 10.1088/0268-1242/15/11/305.
- [10] N. Al Saqri *et al.*, “Investigation of the effects of gamma radiation on the electrical properties of dilute GaAs<sub>1-x</sub>N<sub>x</sub> layers grown by Molecular Beam Epitaxy,” *Curr. Appl. Phys.*, vol. 15, no. 10, pp. 1230–1237, 2015, doi: 10.1016/j.cap.2015.07.010.
- [11] M. Al Huwayz *et al.*, “Effects of substrate material on the electrical properties of self-assembled InAs quantum dots-based laser structures,” *Appl. Phys. A*, vol. 129, no. 6, p. 405, Jun. 2023, doi: 10.1007/s00339-023-06626-w.
- [12] M. Al Huwayz *et al.*, “Optical properties of self-assembled InAs quantum dots based P–I–N structures grown on GaAs and Si substrates by Molecular Beam Epitaxy,” *J. Lumin.*, vol. 251, no. February, 2022, doi: 10.1016/j.jlumin.2022.119155.
- [13] S. Alhassan *et al.*, “Investigation of the effect of substrate orientation on the structural, electrical and optical properties of n-type GaAs<sub>1-x</sub>Bi<sub>x</sub> layers grown by Molecular Beam Epitaxy,” *J. Alloys Compd.*, vol. 885, 2021, doi: 10.1016/j.jallcom.2021.161019.
- [14] Ö. Güllü, F. Demir, F. E. Cimilli, and M. Biber, “ $\gamma$ -Irradiation-induced changes at the electrical characteristics of Sn/p-Si Schottky contacts,” *Vacuum*, vol. 82, no. 8, pp. 789–793, 2008, doi: 10.1016/j.vacuum.2007.11.006.
- [15] S. F. Chung, T. C. Wen, and A. Gopalan, “Influence of dopant size on the junction properties of polyaniline,” *Mater. Sci. Eng. B Solid-State Mater. Adv. Technol.*, vol. 116,

no. 2, pp. 125–130, 2005, doi: 10.1016/j.mseb.2004.09.023.

View Article Online  
DOI: 10.1039/D3CP03865C

- [16] J. H. Werner, “Schottky barrier and pn-junction I/V plots - Small signal evaluation,” *Appl. Phys. A Solids Surfaces*, vol. 47, no. 3, pp. 291–300, 1988, doi: 10.1007/BF00615935.
- [17] T. Gu, M. A. El-Emawy, K. Yang, A. Stintz, and L. F. Lester, “Resistance to edge recombination in GaAs-based dots-in-a-well solar cells,” *Appl. Phys. Lett.*, vol. 95, no. 26, 2009, doi: 10.1063/1.3277149.
- [18] H. F. Lu, L. Fu, G. Jolley, H. H. Tan, S. R. Tatavarti, and C. Jagadish, “Temperature dependence of dark current properties of InGaAs/GaAs quantum dot solar cells,” *Appl. Phys. Lett.*, vol. 98, no. 18, 2011, doi: 10.1063/1.3586251.
- [19] A. B. M. H. Islam, D. S. Shim, and J. I. Shim, “Enhanced radiative recombination rate by local potential fluctuation in InGaN/AlGaN near-ultraviolet light-emitting diodes,” *Appl. Sci.*, vol. 9, no. 5, 2019, doi: 10.3390/app9050871.
- [20] N. I. Bochkareva *et al.*, “Defect-related tunneling mechanism of efficiency droop in III-nitride light-emitting diodes,” *Appl. Phys. Lett.*, vol. 96, no. 13, 2010, doi: 10.1063/1.3367897.
- [21] B. Şahin, H. Çetin, and E. Ayyıldız, “The effect of series resistance on capacitance-voltage characteristics of Schottky barrier diodes,” *Solid State Commun.*, vol. 135, no. 8, pp. 490–495, 2005, doi: 10.1016/j.ssc.2005.05.050.
- [22] M. A. Ebeoğlu, F. Temurtas, and Z. Z. Öztürk, “Ag/n-GaAs schottky mis diodes with surface insulating layers prepared using (NH<sub>4</sub>)<sub>2</sub>S solutions without water,” *Solid. State. Electron.*, vol. 42, no. 1, pp. 23–27, 1998.
- [23] R. T. Tung, J. P. Sullivan, and F. Schrey, “On the inhomogeneity of Schottky barriers,” *Mater. Sci. Eng. B*, vol. 14, no. 3, pp. 266–280, 1992, doi: 10.1016/0921-5107(92)90309-W.

- [24] E. Rhoderick and R. Williams, *Metal-Semiconductor Contacts*. 1988. Clarendon Press, 1988. View Article Online  
DOI: 10.1039/D3CP03865C
- [25] A. Chitnis *et al.*, “High-quality p-n junctions with quaternary AlInGaN/InGaN quantum wells,” *Appl. Phys. Lett.*, vol. 77, no. 23, pp. 3800–3802, 2000, doi: 10.1063/1.1331084.
- [26] P. Zukowski, J. Partyka, and P. Węgierek, “Effect of ion implantation and annealing on the dielectric properties of silicon,” *Phys. Status Solidi Appl. Res.*, vol. 159, no. 2, pp. 509–515, 1997, doi: 10.1002/1521-396X(199702)159:2<509::AID-PSSA509<3.0.CO;2-K.
- [27] M. Nishiguchi *et al.*, “Radiation tolerant GaAs MESFET with a highly-doped thin active layer grown by OMVPE,” *IEEE Trans. Nucl. Sci.*, vol. 37, no. 6, pp. 2071–2075, 1990, doi: 10.1109/23.101231.
- [28] Ş. Karataş, A. Türüt, and Ş. Altındal, “Effects of  $^{60}\text{Co}$   $\gamma$ -ray irradiation on the electrical characteristics of Au/n-GaAs (MS) structures,” *Nucl. Instruments Methods Phys. Res. Sect. A Accel. Spectrometers, Detect. Assoc. Equip.*, vol. 555, no. 1–2, pp. 260–265, 2005, doi: 10.1016/j.nima.2005.09.017.
- [29] D. A. Jameel, “Electrical performance of organic/inorganic hybrid solar cell devices based on n-type GaAs substrate orientations and a conjugated polymer (PANI),” *Appl. Phys. A*, vol. 127, no. 7, 2021, doi: 10.1007/s00339-021-04718-z.
- [30] D.V.Lang, “Deep-level transient spectroscopy: A new method to characterize traps in semiconductors,” *J. Appl. Phys.*, vol. 45, p. 3023, 1974.
- [31] L. Dobaczewski, A. R. Peaker, and K. Bonde Nielsen, “Laplace-transform deep-level spectroscopy: The technique and its applications to the study of point defects in semiconductors,” *J. Appl. Phys.*, vol. 96, no. 9, pp. 4689–4728, 2004, doi: 10.1063/1.1794897.
- [32] K. Yokota, H. Kuchii, K. Nakamura, M. Sakaguchi, H. Takano, and Y. Ando, “EL2,

- EL3, and EL6 defects in GaAs highly implanted with sulfur,” *J. Appl. Phys.*, vol. 88, no. 9, p. 5017, 2000, doi: 10.1063/1.1315331. View Article Online  
DOI: 10.1039/D3CP03865C
- [33] N. P. Khuchua, L. V. Khvedelidze, M. G. Tigishvili, N. B. Gorev, E. N. Privalov, and I. F. Kodzhespirova, “Deep-level effects in GaAs microelectronics: A review,” *Russ. Microelectron.*, vol. 32, no. 5, pp. 257–274, 2003, doi: 10.1023/A:1025528416032.
- [34] R. Yakimova, T. Paskova, and C. Hardalov, “Behavior of an EL5-like defect in metalorganic vapor-phase epitaxial GaAs:Sb,” *J. Appl. Phys.*, vol. 74, no. 10, pp. 6170–6173, 1993, doi: 10.1063/1.355184.
- [35] D. V. Lang, A. Y. Cho, A. C. Gossard, M. Ilegems, and W. Wiegmann, “Study of electron traps in n-GaAs grown by molecular beam epitaxy,” *J. Appl. Phys.*, vol. 47, no. 6, pp. 2558–2564, 1976, doi: 10.1063/1.322974.
- [36] P. Blood and J. J. Harris, “Deep states in GaAs grown by molecular beam epitaxy,” *J. Appl. Phys.*, vol. 56, no. 4, pp. 993–1007, 1984, doi: 10.1063/1.334040.

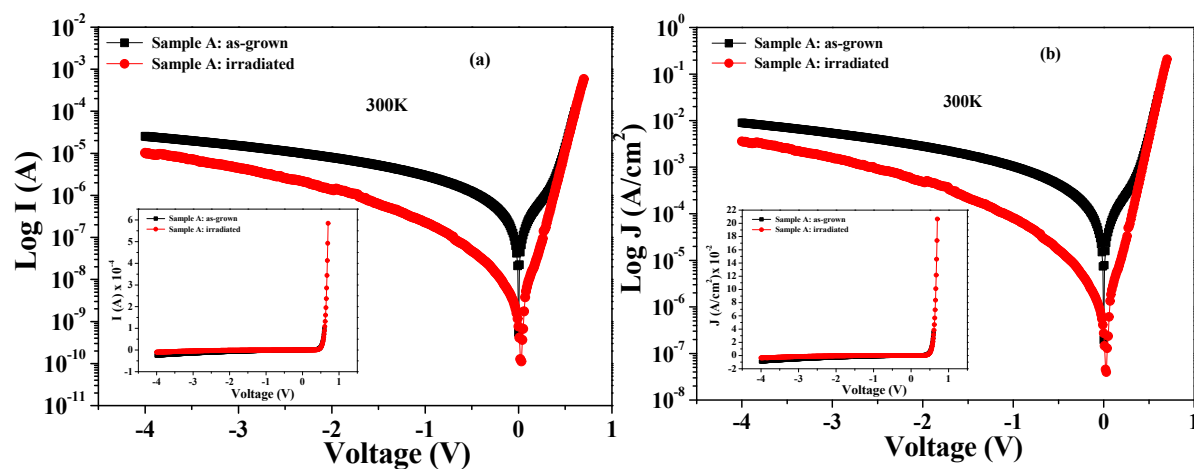


**Figure 1:** (a) Room temperature semi-log plot (I-V) characteristics of Sample A: as-grown and irradiated. (b) Semi-log plot (J-V) characteristics of Sample A: as-grown and irradiated with the same area of  $A = 2.83 \times 10^{-3} \text{ cm}^2$ . The insets in (a) and (b) show a linear I-V plot and a linear J-V plot, respectively.

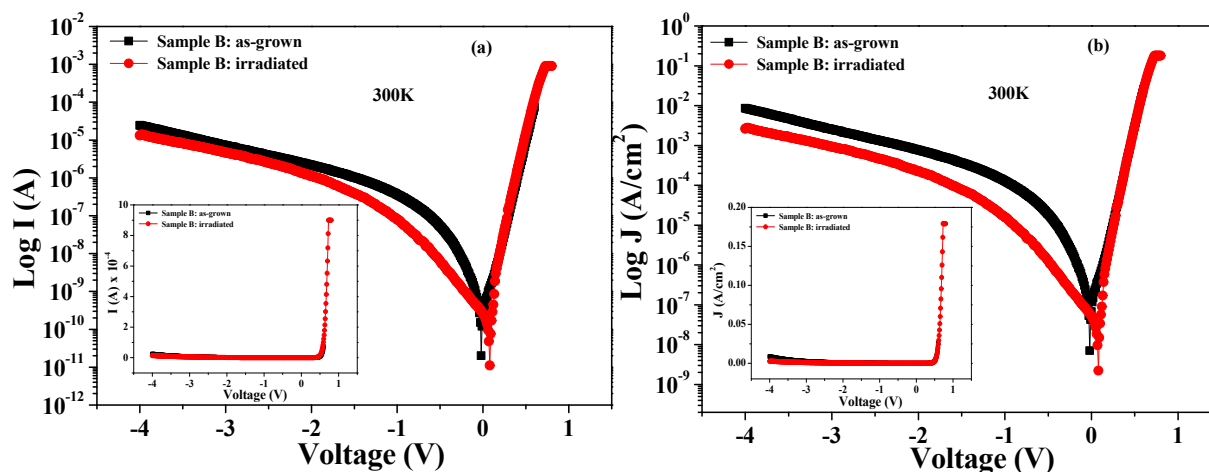


**Figure 2:** (a) Room temperature semi-log plot (I-V) characteristics for Sample B: as-grown and irradiated. (b) Room temperature Semi-log plots of dark J-V characteristics for Sample B: as-grown ( $A = 2.83 \times 10^{-3} \text{ cm}^2$ ) and irradiated ( $A = 5.02 \times 10^{-3} \text{ cm}^2$ ). The insets in (a) and (b) show a linear I-V plot and a linear J-V plot, respectively.

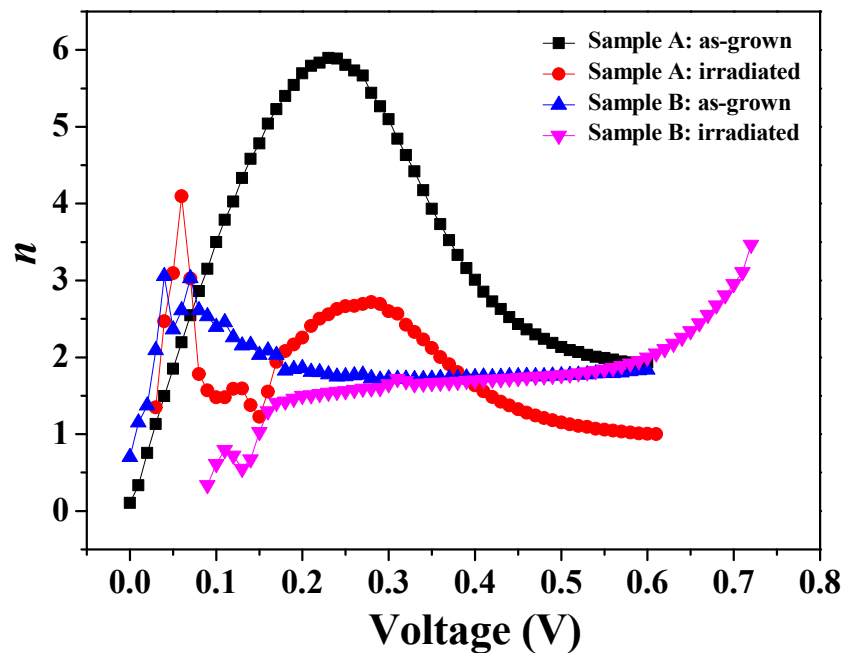


**Figure 3:** Voltage dependence of the local ideality factor for as-grown and irradiated Sample A and Sample B at 300 K.

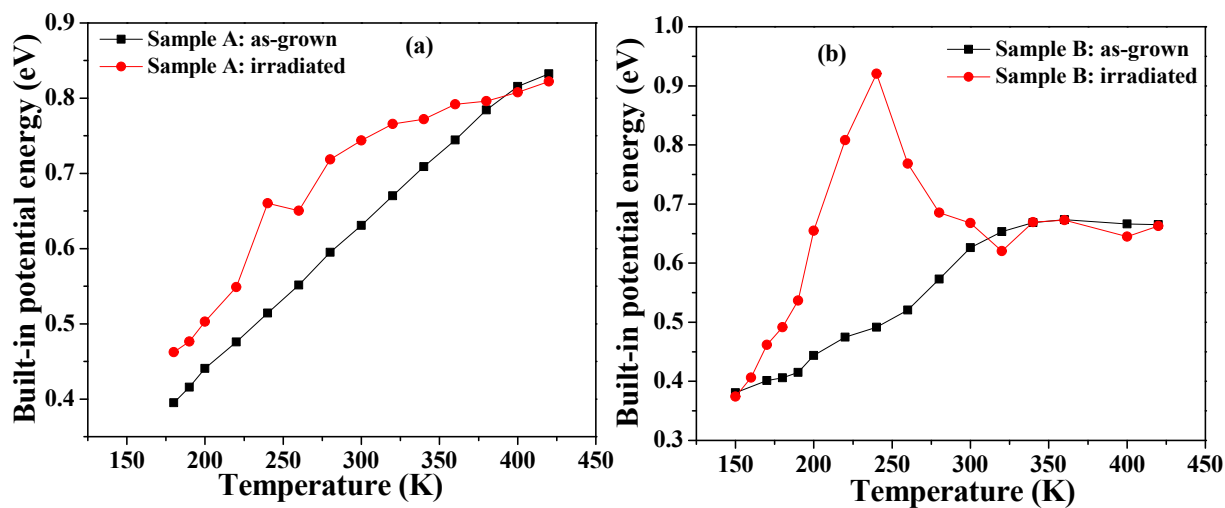


**Figure 4:** Temperature dependence of the experimental built-in potential energy of as-grown and gamma irradiated: (a) Sample A; (b) Sample B.

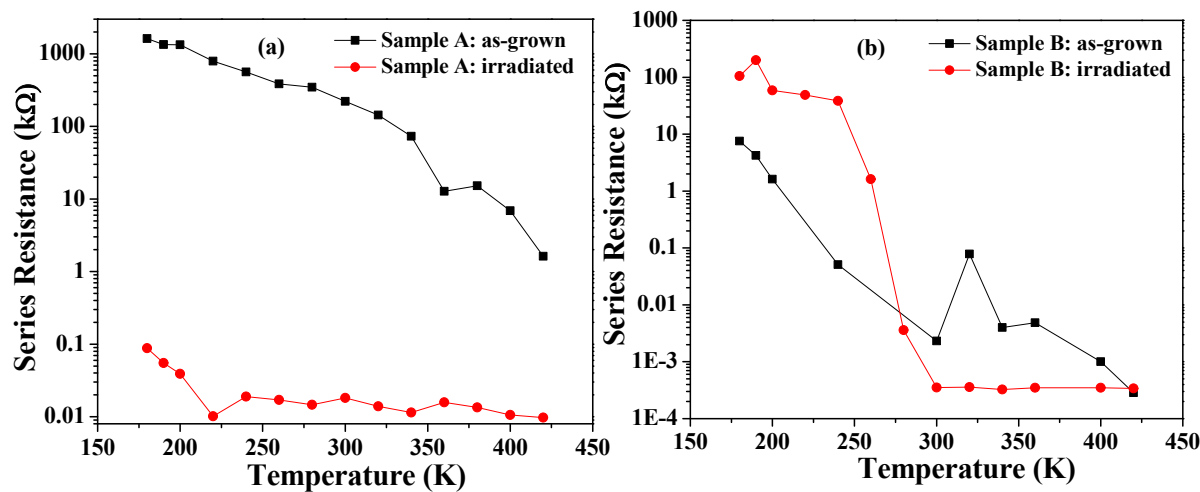


**Figure 5:** Temperature dependence of the experimental series resistance determined from I–V characteristics of as-grown and gamma irradiated: (a) Sample A; (b) Sample B. It is important to note that the as-grown sample has a smaller area than the irradiated sample.

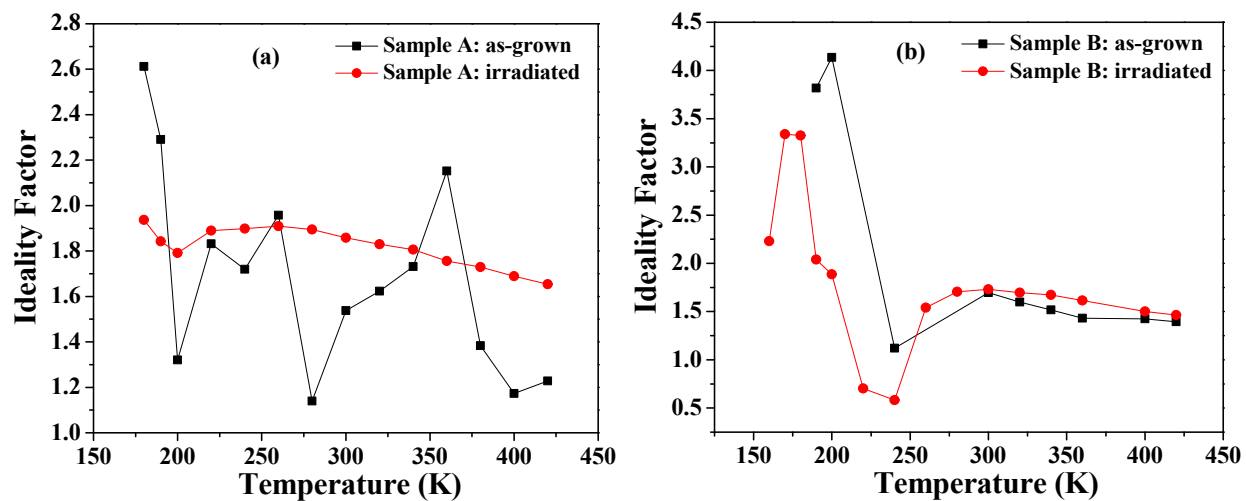


**Figure 6:** Temperature dependence of the experimental ideality factor of as-grown and gamma irradiated: (a) Sample A; (b) Sample B.

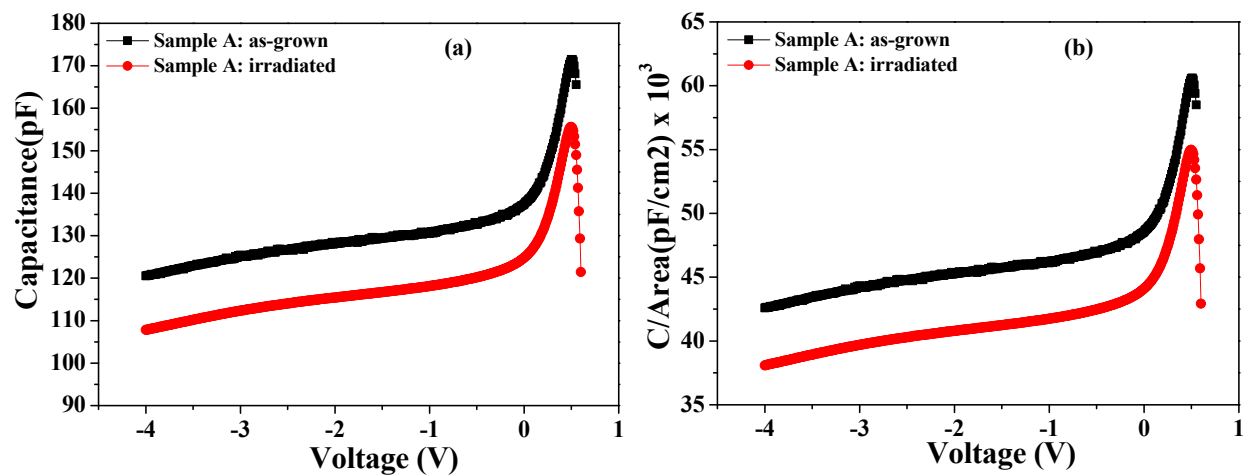


**Figure 7:** (a) Variation of capacitance  $C$  versus reverse bias  $V$  at room temperature for Sample A: as-grown and irradiated. (b)  $C/\text{Area}-V$  characteristics for Sample A: as-grown ( $A = 2.83 \times 10^{-3} \text{ cm}^2$ ) and irradiated ( $A = 2.83 \times 10^{-3} \text{ cm}^2$ ).

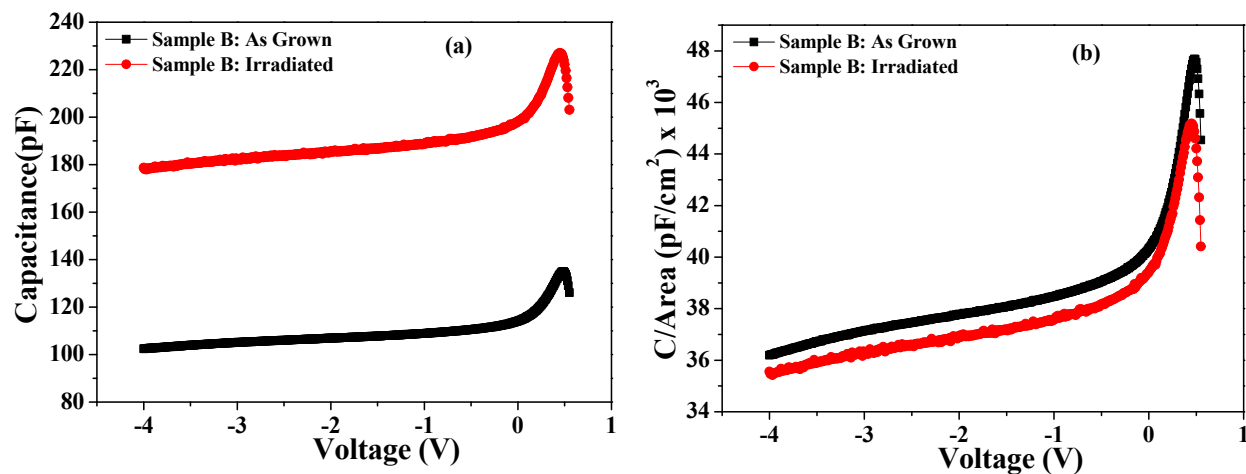


**Figure 8:** (a) Variation of capacitance  $C$  versus reverse bias  $V$  at room temperature for Sample B: as-grown and irradiated. (b)  $C/\text{Area}-V$  characteristics for Sample B: as-grown ( $A = 2.83 \times 10^{-3} \text{ cm}^2$ ) and irradiated ( $A = 5.02 \times 10^{-3} \text{ cm}^2$ ).

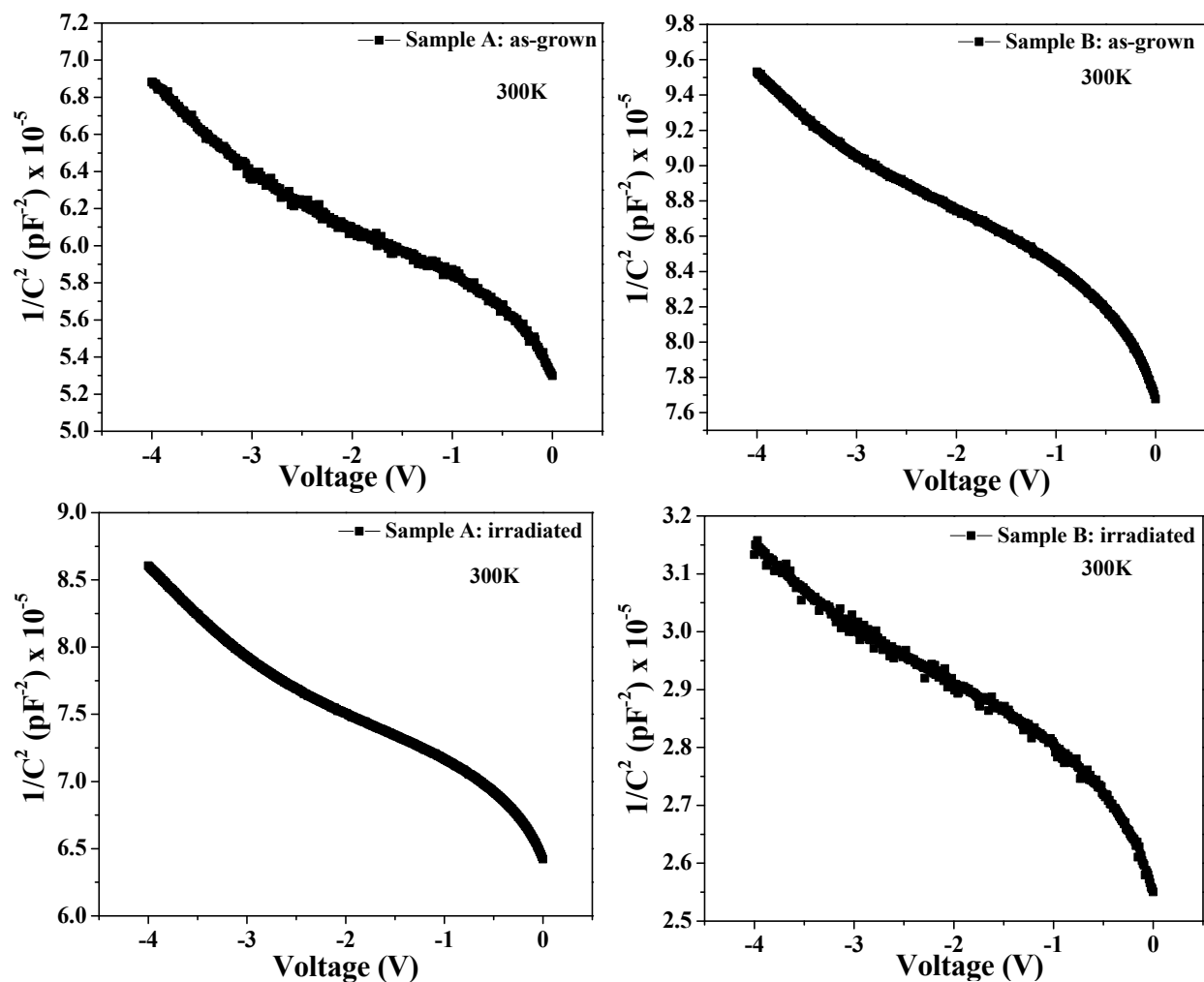


**Figure 9:** Plots of  $1/C^2$  versus V for both as-grown and irradiated samples at room temperature. The solid lines represent the best fit to the data points.

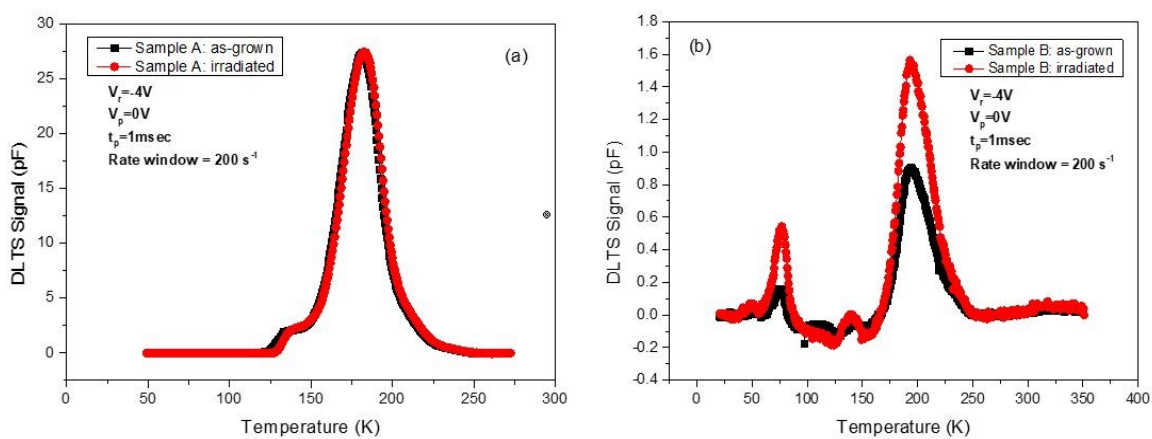


**Figure 10:** DLTS spectra of as-grown and irradiated: (a) Sample A and (b) Sample B at  $V_R = -4V$

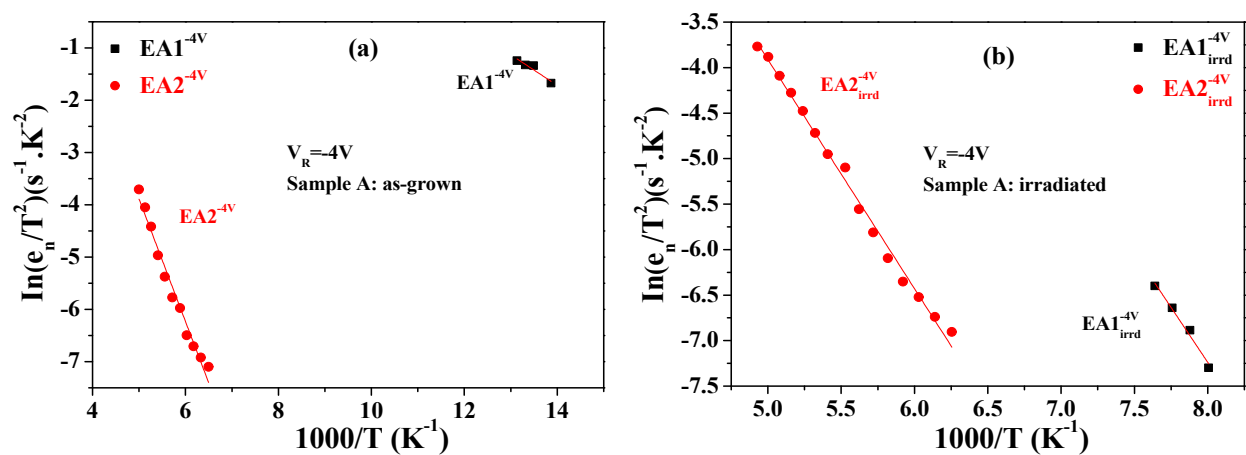


**Figure 11:** Arrhenius plots obtained from Laplace DLTS spectra with reverse biases  $V_R = -4\text{V}$ , filling pulse height  $V_p = 0\text{V}$ , and filling pulse time  $t_p = 1$  msec. For Sample A (a) as-grown and (b) after irradiation. The labelling A and E refer to Sample A (before and after irradiation) and electron traps, respectively. The solid lines represent the best fit to the data points.

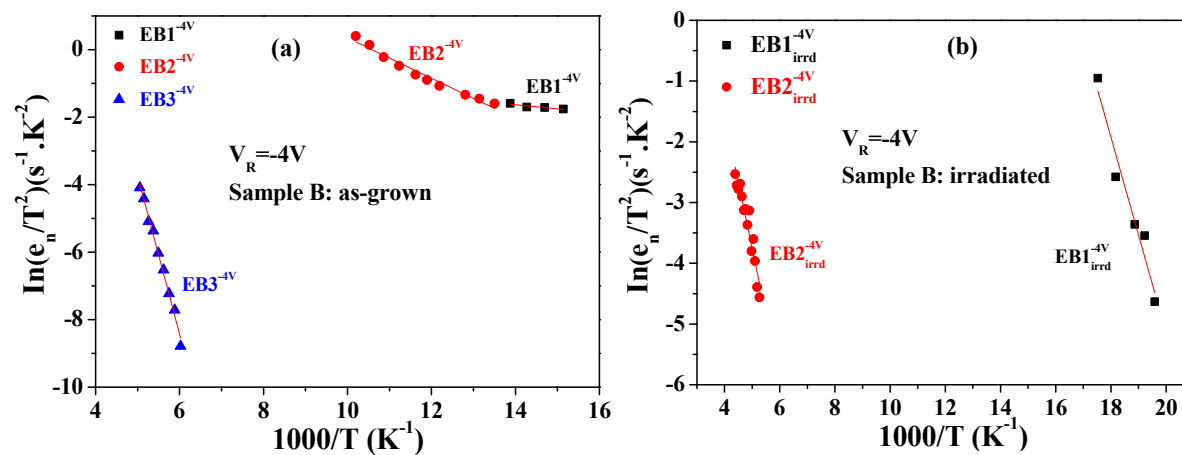


**Figure 12:** Arrhenius plots obtained from Laplace DLTS spectra with reverse biases  $V_R = -4\text{V}$ , filling pulse height  $V_p = 0\text{V}$ , and filling pulse time  $t_p = 1$  msec. For Sample B (a) as grown and (b) after irradiation. The labelling B and E refer to Sample B (before and after irradiation) and electron traps, respectively. The solid lines represent the best fit to the data points.

**Table 1** Ideality factor ( $n$ ), built-in potential energy ( $V_{bi}$ ) and series resistance ( $R_s$ ) at room temperature for Samples A and B: as-grown and irradiated. It is important to note that as-grown Sample B has a smaller area than irradiated Sample B.

Sample ID	$n$	$V_{bi}$ (eV)	$R_s$ (k $\Omega$ )
Sample A: as-grown	1.54	0.63	221.58
Sample A: irradiated	1.86	0.74	$20 \times 10^{-3}$
Sample B: as-grown	1.70	0.63	$2.31 \times 10^{-3}$
Sample B: irradiated	1.73	0.67	$3.5 \times 10^{-4}$

**Table 1 2** Activation energy, capture cross-section, and concentration of the detected traps in Sample A before and after irradiation at ( $V_R = -4$  V,  $V_p = 0$  V) with  $t_p = 1$  msec and rate window =  $200$  s<sup>-1</sup>.

Sample ID	Reverse Bias (V)	Trap	Activation Energy (eV)	Trap Concentration (cm <sup>-3</sup> )	Capture Cross-section $\sigma_\infty$ (cm <sup>2</sup> )
Sample A as-grown	-4	EA1 <sup>-4V</sup>	0.05 ± 0.01	7.58 × 10 <sup>14</sup>	3.02 × 10 <sup>-18</sup>
		EA2 <sup>-4V</sup> (EL5) [31]	0.45 ± 0.08	2.7 × 10 <sup>16</sup>	2.87 × 10 <sup>-17</sup>
Sample A irradiated	-4	EA1 <sub>irrd</sub> <sup>-4V</sup> (EL10) [32]	0.21 ± 0.02	7.60 × 10 <sup>15</sup>	8.10 × 10 <sup>-16</sup>
		EA2 <sub>irrd</sub> <sup>-4V</sup> (EL10) [32]	0.22 ± 0.01	1.52 × 10 <sup>17</sup>	3.23 × 10 <sup>-17</sup>

**Table 1 3** Activation energy, capture cross-section, and concentration of the detected traps in Sample B before and after irradiation at ( $V_R = -4$  V,  $V_p = 0$  V) with  $t_p = 1$  msec and rate window=200 s<sup>-1</sup>.

Sample ID	Reverse Bias (V)	Trap	Activation Energy (eV)	Trap Concentration (cm <sup>-3</sup> )	Capture Cross-section $\sigma_\infty$ (cm <sup>2</sup> )
Sample B as-grown	-4	EB1 <sup>-4V</sup>	0.0030 ± 0.0002	4.96 × 10 <sup>15</sup>	2.12 × 10 <sup>-17</sup>
		EB2 <sup>-4V</sup>	0.067 ± 0.003	8.54 × 10 <sup>15</sup>	1.8 × 10 <sup>-17</sup>
		EB3 <sup>-4V</sup> (EL5) [31]	0.41 ± 0.01	3.3 × 10 <sup>15</sup>	3.9 × 10 <sup>-20</sup>
Sample B irradiated	-4	EB1 <sub>irrd</sub> <sup>-4V</sup> (EL10)[32]	0.14 ± 0.02	6.94 × 10 <sup>14</sup>	2.73 × 10 <sup>-20</sup>
		EB2 <sub>irrd</sub> <sup>-4V</sup> (EL10)[32]	0.22 ± 0.02	6.58 × 10 <sup>15</sup>	3.24 × 10 <sup>-18</sup>